



**HAL**  
open science

## The effect of ion irradiation on the dissolution of UO<sub>2</sub> and UO<sub>2</sub>-based simulant fuel

Aleksej Popel, Thomas Wietsma, Mark Engelhard, Alan Lea, Odeta Qafoku,  
Clara Grygiel, Isabelle Monnet, Eugene Ilton, Mark Bowden, Ian Farnan

► **To cite this version:**

Aleksej Popel, Thomas Wietsma, Mark Engelhard, Alan Lea, Odeta Qafoku, et al.. The effect of ion irradiation on the dissolution of UO<sub>2</sub> and UO<sub>2</sub>-based simulant fuel. *Journal of Alloys and Compounds*, 2018, 735, pp.1350-1356. 10.1016/j.jallcom.2017.11.216 . hal-02459512

**HAL Id: hal-02459512**

**<https://hal.science/hal-02459512>**

Submitted on 22 May 2024

**HAL** is a multi-disciplinary open access archive for the deposit and dissemination of scientific research documents, whether they are published or not. The documents may come from teaching and research institutions in France or abroad, or from public or private research centers.

L'archive ouverte pluridisciplinaire **HAL**, est destinée au dépôt et à la diffusion de documents scientifiques de niveau recherche, publiés ou non, émanant des établissements d'enseignement et de recherche français ou étrangers, des laboratoires publics ou privés.



Distributed under a Creative Commons Attribution 4.0 International License



## The effect of ion irradiation on the dissolution of UO<sub>2</sub> and UO<sub>2</sub>-based simulant fuel

Aleksej J. Popel<sup>a,b,\*</sup>, Thomas W. Wietsma<sup>c</sup>, Mark H. Engelhard<sup>c</sup>, Alan S. Lea<sup>c</sup>, Odeta Qafoku<sup>d</sup>, Clara Grygiel<sup>e</sup>, Isabelle Monnet<sup>e</sup>, Eugene S. Ilton<sup>d</sup>, Mark E. Bowden<sup>c</sup>, Ian Farnan<sup>a</sup>

<sup>a</sup> Department of Earth Sciences, University of Cambridge, Downing Street, Cambridge, CB2 3EQ, UK

<sup>b</sup> Department of Materials, Imperial College London, London, SW7 2AZ, UK

<sup>c</sup> EMSL, Pacific Northwest National Laboratory, Richland, WA 99352, USA

<sup>d</sup> Pacific Northwest National Laboratory, Richland, WA 99352, USA

<sup>e</sup> CIMAP, CEA-CNRS-ENSICAEN-Université de Caen, BP 5133, 14070, Caen, Cedex 5, France

### ARTICLE INFO

#### Article history:

Received 15 August 2017

Received in revised form

15 November 2017

Accepted 19 November 2017

Available online 21 November 2017

#### Keywords:

UO<sub>2</sub>

Simfuel

Ion irradiation

Radiation damage

Dissolution

Secondary phases

### ABSTRACT

The aim of this work was to study the separate effect of fission fragment damage on the dissolution of simulant UK advanced gas-cooled reactor nuclear fuel in water. Plain UO<sub>2</sub> and UO<sub>2</sub> samples, doped with inactive fission products to simulate 43 GWd/tU of burn-up, were fabricated. A set of these samples were then irradiated with 92 MeV <sup>129</sup>Xe<sup>23+</sup> ions to a fluence of  $4.8 \times 10^{15}$  ions/cm<sup>2</sup> to simulate the fission damage that occurs within nuclear fuels. The primary effect of the irradiation on the UO<sub>2</sub> samples, observed by scanning electron microscopy, was to induce a smoothening of the surface features and formation of hollow blisters, which was attributed to multiple overlap of ion tracks. Dissolution experiments were conducted in single-pass flow-through (SPFT) mode under anoxic conditions (<0.1 O<sub>2</sub> ppm in Ar) to study the effect of the induced irradiation damage on the dissolution of the UO<sub>2</sub> matrix with data collection capturing six minute intervals for several hours. These time-resolved data showed that the irradiated samples showed a higher initial release of uranium than unirradiated samples, but that the uranium concentrations converged towards  $\sim 10^{-9}$  mol/l after a few hours. Apart from the initial spike in uranium concentration, attributed to irradiation induced surficial micro-structural changes, no noticeable difference in uranium chemistry as measured by X-ray electron spectroscopy or 'effective solubility' was observed between the irradiated, doped and undoped samples in this work. Some secondary phase formation was observed on the surface of UO<sub>2</sub> samples after the dissolution experiment.

© 2017 The Authors. Published by Elsevier B.V. This is an open access article under the CC BY license (<http://creativecommons.org/licenses/by/4.0/>).

### 1. Introduction

Some countries have decided or are positioning themselves to decide in favour of complete or partial geological disposal of spent nuclear fuel (SNF) [1]. A safety case assessment of any geological repository for SNF requires the prediction of the release rates of radioactive elements from the fuel once the containers fail and contact with groundwater is established [2,3]. As a result, extensive work is devoted to studying the different parameters relevant to the dissolution of spent nuclear fuel under geological disposal

conditions [1–14]. However, there are still some aspects that require further clarification.

For example, to the best of our knowledge there is only one publication in the open literature, produced by Matzke [7], which considers the effect of radiation damage on the dissolution of uranium dioxide matrix in water. About 80% (~170 MeV) of the energy liberated in a nuclear fission event is given to fission fragments as kinetic energy which is transformed into heat by their interaction with the crystal electrons and the crystal atoms in the fuel matrix [15]. This results in fission damage which is manifested in lattice parameter increase and lattice strain, surface fission tracks, high burn-up structure, enhanced diffusion, and creep, leading to the degradation of the fuel's properties [16–19].

Another important aspect receiving limited attention is the dissolution of the high burn-up structure [4,10–13]. The high burn-

\* Corresponding author. Present address: Department of Earth Sciences, University of Cambridge, Downing Street, Cambridge, CB2 3EQ, United Kingdom.

E-mail address: [apopel@cantab.net](mailto:apopel@cantab.net) (A.J. Popel).

up structure is a scientifically interesting and technologically important phenomenon [20]. Fuel pellets with an average burn-up above ~45 GWd/tU [19] show a crystallographic restructuring at the peripheral region, called the 'rim structure' or 'high burn-up structure' [21]. This structure is characterized by the existence of highly dense sub-grains with a size of around 100 nm and the accumulation of pores with an average size of about 1  $\mu\text{m}$  [21]. This restructuring can influence the fuel performance by affecting fission gas release, fuel temperature, hardness, and swelling [21]. The high concentration of fission products and plutonium together with the small grain size near the surface of the fuel pellet are of concern for spent nuclear fuel storage and geological disposal since upon water exposure, leaching starts in this region, which has the highest radiotoxicity [20]. Thus, the high burn-up structure has been studied widely [18,21–35]. However, the exact mechanism, the kinetics and the extent of its formation are still unclear [19,23,25,29].

Dissolution rate and solubility of uranium dioxide in aqueous environments are strongly dependent on uranium oxidation state, as  $\text{U}^{6+}$  is more soluble than  $\text{U}^{4+}$  by several orders of magnitude [36]. As a result, oxidation of  $\text{UO}_2$  increases its solubility by almost five orders of magnitude [37]. Another key factor that determines the kinetics of uranium dioxide dissolution is its solid-state conductivity, where the dissolution rate increases with electrical conductivity of the  $\text{UO}_2$  matrix [2,3]. Nakae et al. [38] showed that the dependence of electrical conductivity of  $\text{UO}_2$  on radiation damage is rather complex, but generally the radiation damage results in a decrease of the electrical conductivity of  $\text{UO}_2$ .

We believe that the complex chemical system produced by accumulated radiation damage is important for understanding the dissolution of the high burn-up structure [4], yet little work has been done in this area. This contribution addresses these knowledge gaps by attempting to quantify the effect of radiation damage by fission-energy ions and dopants, which simulate fission products, on the aqueous dissolution of the spent fuel  $\text{UO}_2$  matrix.

For this purpose, plain  $\text{UO}_2$  and  $\text{UO}_2$ -based simulant fuel (sim-fuel) (43 GWd/tU simulated burn-up) bulk polycrystalline samples were produced and irradiated with 92 MeV  $^{129}\text{Xe}^{23+}$  ions to a fluence of  $4.8 \times 10^{15}$  ions/ $\text{cm}^2$ . The irradiated and unirradiated samples were analysed by scanning electron microscopy (SEM), including dual beam SEM-FIB (focused ion beam) set-up, atomic force microscopy (AFM), and X-ray photoelectron spectroscopy (XPS). Single-pass flow-through dissolution experiments under an anoxic atmosphere (<0.1 ppm  $\text{O}_2$  in Ar) were then conducted in deionised water to determine the effect of dopants and radiation damage on aqueous durability. The uranium concentration in the sampled solutions was determined by inductively-coupled plasma mass spectrometry (ICP-MS). Following the dissolution experiments, changes to the surface of the samples were characterized using SEM and XPS techniques.

## 2. Experimental details

### 2.1. Sample production and irradiation

The sample fabrication was conducted and described by Hiez et al. in Ref. [39]. Thirteen stable elements were added in the form of oxides and carbonates to depleted  $\text{UO}_2$  (0.3 wt%  $^{235}\text{U}$ ) to simulate the composition of spent fuel after burn-up of 43 GWd/tU and, as a reference, pure  $\text{UO}_2$  samples were also prepared. The dopant blends were homogenised with  $\text{UO}_2$  powder. The compacted pellets were sintered at 1730 °C in an atmosphere of 99.5 vol%  $\text{H}_2$  and 0.5 vol%  $\text{CO}_2$  for 300 min to produce the samples with densities of 10.69 (plain  $\text{UO}_2$ ) and 9.74  $\text{g}/\text{cm}^3$  (simulated 43 GWd/tU). The pellets were cut into discs with a diameter 9.4–9.5 mm and a thickness ca.

1 mm using a diamond saw. The activity of the discs was in the range of 6–8 kBq, hence these samples had to be treated as radioactive material in compliance with the relevant regulations. The samples were cut and stored under an ambient air atmosphere.

Ion irradiation was conducted to simulate the radiation damage produced by fission fragments during in-reactor fuel irradiation. The xenon irradiation was performed with 92 MeV  $^{129}\text{Xe}^{23+}$  ions to a fluence of  $4.8 \times 10^{15}$  ions/ $\text{cm}^2$  at a flux of ca.  $1.3 \times 10^{10}$  ions/( $\text{cm}^2$  s), which caused heating of the samples to a temperature not exceeding 150 °C on the IRRSUD beamline at the GANIL accelerator, Caen, France. The Xe ions used in this work are representative of typical fission fragments in terms of energy [40] and mass [41]. The irradiations were conducted at an ambient temperature of ca. 19 °C. The temporal structure of the ion beam was 1 ns ion pulse every 100 ns (due to the nature of cyclotron) and the beam was swept across the surface of the samples with a frequency of 400 Hz in the horizontal and 4 Hz in the vertical direction to ensure homogenous irradiation. According to the SRIM-2013.00 software [42], the expected initial nuclear and electronic stopping,  $dE/dx$ , for 92 MeV Xe ions in  $\text{UO}_2$  is 0.26 and 24.6 keV/nm, respectively, and the projected ion range is ~6.5  $\mu\text{m}$ . A theoretical  $\text{UO}_2$  density of 10.96  $\text{g}/\text{cm}^3$  [43] was assumed in this SRIM calculation.

### 2.2. Sample characterisation

The SEM analyses were performed on a FEI Quanta 3D FEG Dual Beam (SEM-FIB) instrument, which contains a focused  $\text{Ga}^+$  ion beam and high resolution field emission scanning electron column. Samples were mounted on a carbon tape before they were loaded into the SEM chamber. The SEM micrographs were collected using secondary electron imaging at a voltage of 5 kV and a current of 0.17–0.68 nA. A gallium ion beam (30 kV, 1 nA) was applied to cut the surface blisters for investigating their internal structure. A Digital Instruments Bioscope II with a NanoScope IV controller was used for AFM studies. Prior to the AFM measurements, the surface of the samples was cleaned first using acetone and subsequently with methanol using cotton swabs. The surface topography was measured utilising the intermittent contact (tapping) mode using silicon cantilevers (K-Tek Tetra15) with a nominal spring constant of 40 N/m, a scan size of  $5 \times 5 \mu\text{m}$  and a scan rate of 1.2 Hz. The image data were subjected to first order flattening, which removes the Z offset and tilt between the scan lines prior to the roughness measurements.

A Kratos Axis Ultra DLD spectrometer with a monochromatic Al  $K_{\alpha}$  X-ray (1486.7 eV) source at 10 mA, 15 kV for excitation was used to perform the XPS measurements. High resolution analyses were carried out with an elliptical analysis area with 300 and 700  $\mu\text{m}$  minor and major axes, respectively, using pass energies of 20 or 40 eV with a step size of 0.1 or 0.125 eV. These conditions produced a full width at half maximum (FWHM) for the Ag  $3d_{5/2}$  line of 0.54 or 0.77 eV, respectively. The energy scale was referenced to adventitious C 1s at 285.0 eV. Standards for U(VI), U(V) and U(IV) were used to determine the satellite structures and primary peak parameters. Both the primary and satellite peaks for U 4f were used in the fitting procedure following the methodology outlined in Ilton et al. [44]. The U(IV) and U(VI) standards were synthetic stoichiometric  $\text{UO}_2(\text{cr})$ , as used by Schofield et al. [45], and schoepite, respectively. The U 4f parameters for U(V) were derived by fitting the U 4f spectrum of a synthetic U(V)-U(VI) oxyhydroxide phase,  $\text{U}(\text{H}_2\text{O})_2(\text{UO}_2)_2\text{O}_4(\text{OH})(\text{H}_2\text{O})_4$ , with the U(VI) standard. The U 4f spectra were best fit after using Shirley background [46] subtractions by non-linear least squares fitting using the CasaXPS curve resolution software.

XRD and TEM studies were performed to assess the effect of the dopants and ion irradiation on the structural properties of the  $\text{UO}_2$

matrix and will be published elsewhere [47].

### 2.3. Dissolution experiments

Dissolution experiments were conducted using a polytetrafluoroethylene continuously stirred tank reactor with a residence volume of 21.7 ml. The Mili-Q deionised water (18.2 M $\Omega$ /cm) was degassed using an online vacuum degassing system and collected in a bottle inside the glove box with a controlled Ar atmosphere ( $O_2 < 0.1$  ppm). The dissolution experiments were performed in the single-pass flow-through mode by placing one sample at a time in the reactor and pumping the prepared deionised water for 10 h. The outlet solution was collected for 5 or 6 min in individual polyethylene vials using an automated sampling system. The volumetric water flow rate was set to 2.0 ml/min resulting in a reactor residence time of 10.9 min and sampled volumes of 10 or 12 ml were taken. The ambient temperature during the dissolution experiments was either 21 or 25 °C. Some of the sampled solutions were transferred into another set of sample vials for ICP-MS analysis and the original samples were left in the glove box for further studies. Some  $UO_2$  samples were left overnight in the dissolution reactor filled with water after the flow-through experiment was completed for overnight batch dissolution. The reactor was cleaned with nitric acid solution and deionised water between different dissolution experiments and its cleanliness was checked by ICP-MS analysis.

The sampled solutions were acidified with 10  $\mu$ l of 15.9 M  $HNO_3$  and uranium concentrations were measured by an Agilent 7500 ICP-MS outside of the glove box. The regular analysis of the 50 ppt U quality control standard showed a maximum error in U concentration of 9%. The measured uranium concentration for the blank runs was ca.  $10^{-10}$  mol/l. Hence, the measurement error of 9% or  $\pm 10^{-10}$  mol/l, whichever is greater, should be applied to the obtained U concentration values. The error bars are not plotted on the dissolution graph below for the sake of clarity as their sizes do not affect the observed trends.

After the dissolution experiment some of the samples were assessed for surface structural and uranium oxidation changes induced by the dissolution using XPS and SEM. The samples were transferred under Ar atmosphere to the XPS spectrometer for analysis after the dissolution experiments.

## 3. Results and discussion

### 3.1. Sample characterisation

Initial characterisation of the as-produced samples was performed by Hiezl et al. and is available in Ref. [39]. SEM (Fig. 1a) and AFM (not shown) characterisation showed that the unirradiated cut disks have a high surface roughness with height variation up to 2.4  $\mu$ m and significant variation (up to three times) between different regions. Occasionally, regions with granular structure (Fig. 1b) were observed with SEM. It is believed that these granular regions correspond to places where gas cavities were cut by the diamond saw. The grains showed wavy surface morphologies, which were also observed by He et al. [37,48] and related to uranium oxides with higher oxygen coefficients. Thus, from Fig. 1b and based on the observations of He et al., it appears that even within the same grain there are regions with different oxygen coefficients and, hence, with different uranium ionic composition.

The Xe ion irradiation smoothed the surface features (Fig. 2a) and caused hollow blisters to form (Fig. 2b). Several randomly selected blisters were cut with  $Ga^+$  ion FIB and were observed to have cavities. Some blisters appeared collapsed (e.g., rear blister in Fig. 2b).

Lozano et al. [29] reported that two types of subgrains are observed in the rim area of a high burn-up fuel (>60 GWd/tU, locally): polyhedral and round. The polyhedral subgrains, up to 0.8  $\mu$ m in size, were attributed to be characteristic of the high burn-up structure, whereas the round subgrains, of about 0.1  $\mu$ m in size, were associated with free surface rearrangement, for example, inside a pore. The irradiation conditions used in this work in terms of the energy and mass of the ions and the attained fluence were very similar to the irradiation conditions used in the work by Baranov et al. [23] and Sonoda et al. [21]. Baranov et al. [23] managed to achieve grain subdivision in bulk  $UO_2$ -based simfuel pellets (simulated 120 GWd/tU) by irradiating with 90 MeV  $Xe^{24+}$  ions to fluences up to  $5 \times 10^{15}$  ions/cm<sup>2</sup> with a flux of  $\sim 5 \times 10^{10}$  ions/(cm<sup>2</sup> s) at room temperature. The size of subgrains was reported to depend on local dislocation density and was in the range of 200 nm to 400 nm along the irradiated surface. Sonoda et al. [21] observed subgrain formation, with a size around 1  $\mu$ m, in bulk  $UO_2$  samples irradiated by 210 MeV  $Xe^{14+}$  ions from a fluence over  $1.0 \times 10^{15}$  ions/cm<sup>2</sup> at room temperature (flux is not reported). Hence, it would be reasonable to expect very similar results from the ion irradiation in our work, although our samples were not polished. Instead we observe smoothing of the surface, as if melting took place, and formation of blisters. Since the initial electronic stopping power of 92 MeV Xe ions is 24.6 keV/nm, which should be sufficient to cause visible ion tracks with a diameter about 2 nm [21], we suggest that the observed microstructure is a result of multiple overlap ( $\sim 150$  times) of ion tracks with the centreline temperature exceeding the melting point of  $UO_2$  (3150 K) [43]. The signs of significant microstructural restructuring were also observed before for  $UO_2$  thin film [49], bulk and thin film  $CeO_2$  [50] samples irradiated under identical conditions.

The aim of the XPS analysis was to examine whether the ion irradiation caused any permanent  $U^{4+}$  ionisation to the higher oxidation states due to electronic excitation during the electronic stopping of the Xe ions in  $UO_2$ . The information depth of the XPS measurement ( $\sim 3$  nm) is such that the study performed on the irradiated and unirradiated samples indicated that the samples were subjected to significant surface oxidation. Since the samples were cut and stored under ambient air atmosphere, surface oxidation has masked potential ion irradiation and doping effects. The oxygen coefficient values were in the range 2.22–2.33, which corresponds to the surface composition from  $UO_{2+x}$  (where  $x < 0.25$ ) to  $U_3O_7$ . The proportion of U(IV), U(V) and U(VI) was in the range 60–44, 36–47, 4–9%, correspondingly. It should be noted that these numbers represent average values over elliptical analysis area with 300 and 700  $\mu$ m minor and major axes, respectively. Similar results were obtained before in Ref. [51] for  $UO_2$  thin film samples irradiated under identical conditions.

### 3.2. Dissolution results

Nine samples were subjected to the time-resolved SPFT dissolution experiment: three unirradiated plain, two irradiated plain, two unirradiated and irradiated doped (simulated 43 GWd/tU) samples. These data reveal a complex behaviour with time largely involving very low levels of U dissolution. Unirradiated samples were expected to release a readily soluble  $U^{6+}$  in the oxidised surface. The main findings of the dissolution study were (Fig. 3): 1) the irradiated samples generally showed a higher initial release of uranium than unirradiated ones; 2) after the initial release, uranium concentrations from different samples (irradiated and unirradiated, doped and plain) converged towards the value of the same order ( $\sim 10^{-9}$  mol/l) with time. No noticeable difference was observed in the dissolution behaviour between the plain and doped (simulated 43 GWd/tU) samples under conditions used in this

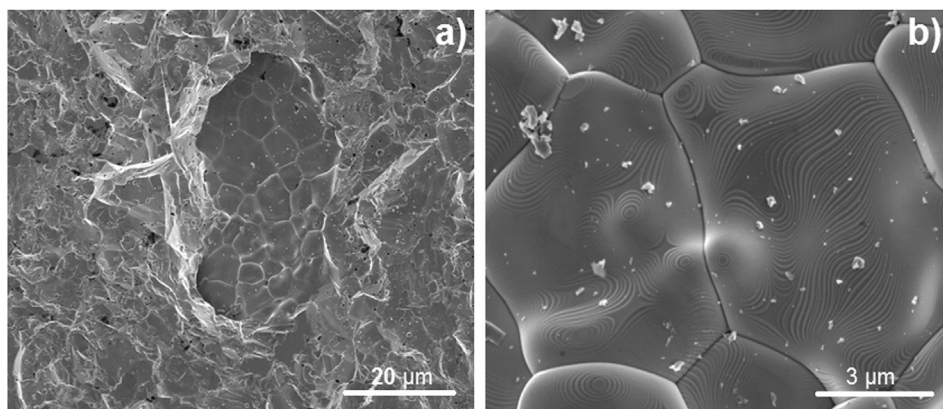


**Fig. 1.** Secondary electron SEM micrographs showing the surface topography of an unirradiated plain  $\text{UO}_2$  sample (s12): a) low magnification image depicts high surface roughness and a region with granular structure b) a high magnification image of the granular region shows wavy surface morphologies.

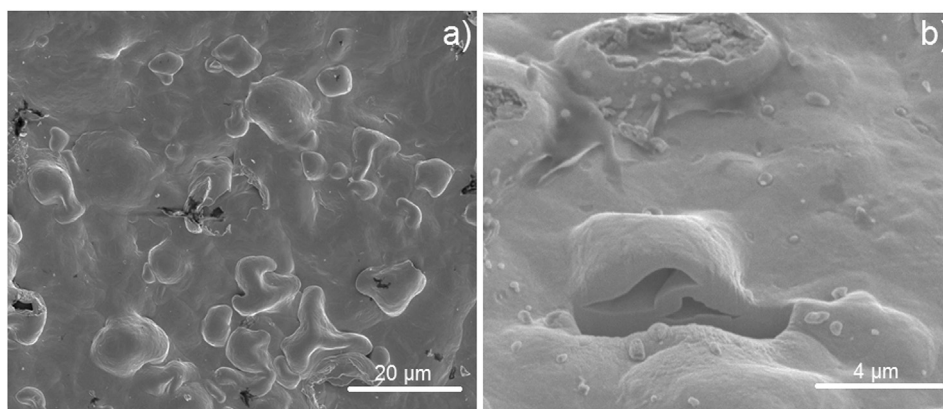


**Fig. 2.** Secondary electron SEM micrographs showing the surface topography of irradiated  $\text{UO}_2$  samples: a) a plain  $\text{UO}_2$  sample with surface smoothing and blisters; b) doped  $\text{UO}_2$  sample (simulated 43 GWd/tU) showing a blister cavity after a FIB cut out.

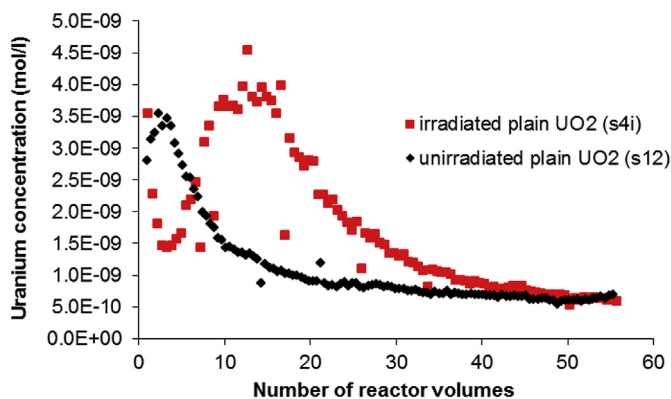


**Fig. 3.** A plot of U concentration as a function of number of reactor volumes for a plain unirradiated (s12) and Xe irradiated (s4i)  $\text{UO}_2$  sample.

work. The initial higher release of uranium from the irradiated samples can be attributed to dissolution of the strained regions due to induced radiation damage. The complex shape of the dissolution curves (rise and fall in concentration values of U) can be explained by water accessing new regions of the  $\text{UO}_2$  surface oxidised in air. In the case of the irradiated sample shown in Fig. 3, collapse of the blisters (Fig. 4a) and subsequent dissolution of the blisters' inner

surface is more likely responsible for its complex dissolution curve. Another plain irradiated sample (s5i) showed a high initial release of uranium ( $4.1 \times 10^{-6}$  mol/l in the first sample, Table 1), which quickly dropped (after 6.5 reactor volumes) to the level of  $\sim 10^{-9}$  mol/l which was maintained until the end of the experiment. This high initial release of uranium is likely associated with a small region of U(VI) present (e.g.,  $\text{UO}_3 \cdot x\text{H}_2\text{O}$ ) on the surface of the sample. It is known that aging of  $\text{UO}_2$  in ambient air might cause the formation of a thin coating of highly oxidised material –  $\text{UO}_3$  or one of its hydrates [52]. Uranium in the  $\text{U}^{6+}$  oxidation state has a solubility of ca.  $10^{-6}$  mol/l in water at neutral pH [3] and demonstrates fast dissolution kinetics [53]. All samples showed an initial rapid release of uranium, caused by an oxidised coating at the surface of the samples, followed by a slow decrease in uranium concentration. This is consistent with previous observations in Ref. [54]. As the surface of the samples gets depleted of strained and oxidised regions, the dissolution behaviour converges towards the same value. It was observed that when the sampled solutions were transferred into other sample vials to be taken out for ICP-MS analysis, consistent dips in the measured uranium concentration values were observed (Fig. 3, sample s4i, reactor volumes 7, 9, 17, 26, 34, 42, 50). It is likely that uranium adsorbs on the surface of the pipette tip and the new vial. This suggestion is also supported by the fact that acid washes of the reactor (Table 1) showed consistently higher measured uranium concentrations than the samples at any other stage of the dissolution experiment. This indicates that

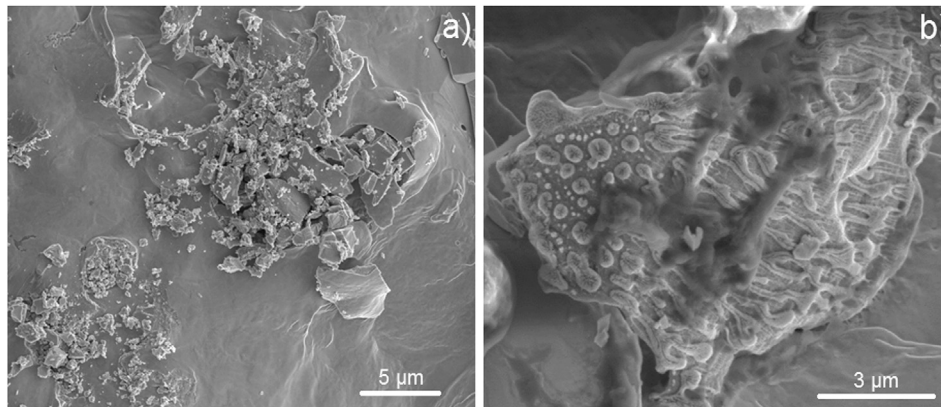


**Fig. 4.** Secondary electron SEM micrographs depicting changes in surface topography of a plain irradiated  $\text{UO}_2$  sample (s4i) after dissolution: a) a collapsed blister; b) circular secondary phase formations.

**Table 1**

Concentration of uranium in different solution sample types for plain irradiated and unirradiated samples.

solution sample type from dissolution of plain $\text{UO}_2$ samples	c(U) (mol/l)		
	s12 ( $\text{UO}_{2.28}$ ), unirradiated	s4i ( $\text{UO}_{2.29}$ ), irradiated	s5i ( $\text{UO}_{2.31}$ ), irradiated
first flow-through sample	$2.8 \times 10^{-9}$	$3.5 \times 10^{-9}$	$4.1 \times 10^{-6}$
last flow-through sample	$6.9 \times 10^{-10}$	$5.9 \times 10^{-10}$	$2.3 \times 10^{-9}$
sample after overnight batch dissolution	$6.7 \times 10^{-9}$	$2.3 \times 10^{-9}$	$4.0 \times 10^{-7}$
sample after reactor acid wash	$1.7 \times 10^{-8}$	$4.1 \times 10^{-7}$	$2.0 \times 10^{-6}$

uranium adsorbs on the surface of the reactor during the dissolution experiment and is consistent with previously observed behaviour [55].

SEM analysis of the samples after the dissolution experiments showed circular secondary phase formations ( $d = 50\text{--}100$  nm) on the surface of sample s4i (Fig. 4b). Further work with sub-micron characterisation is required to identify this secondary phase, but its solubility must be lower than  $\sim 2 \times 10^{-9}$  (Table 1) so that it can precipitate out of the solution. The only viable candidates for the secondary phase are semi-crystalline  $\text{UO}_2$  or  $\text{UO}_{2+x}$  phases [14,56,57], as the dissolution took place in deionised water at an ambient temperature of  $24\text{--}25$  °C (contact time with water was only 26 h: 8 h in a flow-through mode, 18 h in a batch mode). XPS analyses (Table 2) of the samples after the dissolution experiments were performed to examine the effect of dissolution on the oxidation state of uranium at the surface of the samples and indicated that contact with water resulted in marginal changes in the relative fraction of uranium ions at the surface of the samples, hence the oxygen coefficient  $k_{\text{O}}$  remained virtually unchanged.

It should be noted that even in the case of irradiated sample s5i, where the highest release of uranium was observed, the thickness of uranium dioxide layer dissolved (based on total uranium dissolution) is estimated as  $\sim 60$  nm, which is well below (two orders of magnitude) the expected Xe ion penetration depth of  $\sim 6.5$   $\mu\text{m}$ .

Geometric surface area and dissolution only from the top surface of the sample disc were conservatively assumed. Since the uranium release values for the unirradiated and irradiated samples converge towards the same value with time, and for the irradiated samples the dissolution of the material with accumulated damage is taking place, it can be concluded that the induced radiation damage does not have a significant effect on the dissolution of the  $\text{UO}_{2+x}$  matrix under anoxic conditions.

The XPS and dissolution results highlight the fact that  $\text{UO}_2$  possesses an exceptional ability to recover the induced radiation damage [40] and suggest that radiation damage aspect in real spent nuclear fuel might not be significant in affecting its aqueous durability. This suggestion is consistent with the dissolution results for high burn-up fuel, where no dissolution enhancement was observed as a result of an increased burn-up which implies an increased accumulation of radiation damage [4,11].

#### 4. Conclusions

The ion irradiation caused significant microstructural rearrangements in the  $\text{UO}_2$  samples: smoothing of the surface features and hollow blisters were observed. Multiple overlap of ion tracks with the centreline temperature exceeding the melting point of  $\text{UO}_2$  was suggested to cause these features. However, the

**Table 2**

Summary of the XPS results for the plain irradiated and unirradiated samples before and after the dissolution experiments.

plain $\text{UO}_2$ samples	U(IV) fraction	U(V) fraction	U(VI) fraction	oxygen coefficient $k_{\text{O}}(\text{UO}_{k_{\text{O}}})$
s12, unirradiated	0.51	0.42	0.07	2.28
s12r	0.50	0.46	0.05	2.28
s4i, irradiated	0.50	0.44	0.07	2.29
s4ir	0.47	0.48	0.05	2.29
s5i, irradiated	0.48	0.45	0.07	2.31
s5ir	0.50	0.44	0.06	2.28

r denotes samples after the dissolution experiments.

underlying  $\text{UO}_2$  surface chemistry as determined by XPS appears unchanged (completely recovered) despite significant electronic disturbance during irradiation.

The dissolution studies showed that the irradiated samples generally showed a higher initial release of uranium than unirradiated ones and, after the initial release, uranium concentrations converged towards the value of the same order ( $\sim 10^{-9}$  mol/l) within a few hours. This result suggests that the induced radiation damage in this work does not have a significant effect on the longer term dissolution of the  $\text{UO}_{2+x}$  matrix under anoxic conditions. Nor was there any noticeable difference in dissolution behaviour between the plain and doped (simulated 43 GWd/tU burn-up) samples under the anoxic conditions used in this work.

Secondary phase formations were observed on the surface of  $\text{UO}_2$  under anoxic dissolution conditions in deionised water at an ambient temperature of 24–25 °C and a contact time with water of only ~26 h. There is a need for sub-micron chemical and structural characterisation of the samples for a better mechanistic understanding of the observed secondary phase formation processes, as well as of the initial oxidation of the  $\text{UO}_2$  creating possible regions of  $\text{UO}_3 \cdot x\text{H}_2\text{O}$  on the surface of the samples after prolonged exposure to air.

### Acknowledgements

The irradiation experiment was performed at the Grand Accélérateur National d'Ions Lourds (GANIL) Caen, France, and supported by the French Network EMIR. The support in planning and execution of the experiment by the CIMAP-CIRIL and the GANIL staff, especially, T. Madi and F. Durantel is much appreciated. Characterisation and dissolution studies were performed using EMSL, a DOE Office of Science User Facility sponsored by the Office of Biological and Environmental Research and located at Pacific Northwest National Laboratory. A.J. Popel acknowledges funding from the UK EPSRC (grant EP/I036400/1 and EP/L018616/1) and Radioactive Waste Management Ltd (formerly the Radioactive Waste Management Directorate of the UK Nuclear Decommissioning Authority, contract NPO004411A-EPS02).

### References

- [1] D. Cui, E. Ekeröth, P. Fors, K. Spahiu, The interaction of dissolved hydrogen with spent fuel or  $\text{UO}_2$  doped with alpha emitters, *Mater. Res. Soc. Symp. Proc.* 1104 (2008).
- [2] D.W. Shoesmith, S. Sunder, The prediction of nuclear fuel ( $\text{UO}_2$ ) dissolution rates under waste disposal conditions, *J. Nucl. Mater.* 190 (1992) 20–35.
- [3] D.W. Shoesmith, Fuel corrosion processes under waste disposal conditions, *J. Nucl. Mater.* 282 (2000) 1–31.
- [4] T. Fanghänel, V.V. Rondinella, J.P. Glatz, T. Wiss, D.H. Wegen, T. Gouder, P. Carbol, D. Serrano-Purroy, D. Papaioannou, Reducing uncertainties affecting the assessment of the long-term corrosion behavior of spent nuclear fuel, *Inorg. Chem.* 52 (2013) 3491–3509.
- [5] M. Amme, T. Wiss, H. Thiele, P. Boulet, H. Lang, Uranium secondary phase formation during anoxic hydrothermal leaching processes of  $\text{UO}_2$  nuclear fuel, *J. Nucl. Mater.* 341 (2005) 209–223.
- [6] T. Mennecart, B. Grambow, M. Fattahi, Z. Andriambololona, Effect of alpha radiolysis on doped  $\text{UO}_2$  dissolution under reducing conditions, *Radiochim. Acta* 92 (2004) 611–615.
- [7] H.J. Matzke, Radiation damage-enhanced dissolution of  $\text{UO}_2$  in water, *J. Nucl. Mater.* 190 (1992) 101–106.
- [8] J. Bruno, I. Casas, I. Puigdomènec, The kinetics of dissolution of  $\text{UO}_2$  under reducing conditions and the influence of an oxidized surface layer ( $\text{UO}_{2+x}$ ): application of a continuous flow-through reactor, *Geochem. Cosmochim. Acta* 55 (1991) 647–658.
- [9] A. Casella, B. Hanson, W. Miller, The effect of fuel chemistry on  $\text{UO}_2$  dissolution, *J. Nucl. Mater.* 476 (2016) 45–55.
- [10] K. Lemmens, E. González-Robles, B. Kienzler, E. Curti, D. Serrano-Purroy, R. Sureda, A. Martínez-Torrents, O. Roth, E. Slonszki, T. Mennecart, I. Günther-Leopold, Z. Hózer, Instant release of fission products in leaching experiments with high burn-up nuclear fuels in the framework of the Euratom project FIRST-Nuclides, *J. Nucl. Mater.* 484 (2017) 307–323.
- [11] D. Serrano-Purroy, F. Clarens, E. González-Robles, J.P. Glatz, D.H. Wegen, J. de Pablo, I. Casas, J. Giménez, A. Martínez-Esparza, Instant release fraction and matrix release of high burn-up  $\text{UO}_2$  spent nuclear fuel: effect of high burn-up structure and leaching solution composition, *J. Nucl. Mater.* 427 (2012) 249–258.
- [12] P. Fors, P. Carbol, S. Van Winckel, K. Spahiu, Corrosion of high burn-up structured  $\text{UO}_2$  fuel in presence of dissolved  $\text{H}_2$ , *J. Nucl. Mater.* 394 (2009) 1–8.
- [13] A.J. Popel, V.G. Petrov, V.A. Lebedev, J. Day, S.N. Kalmykov, R. Springell, T.B. Scott, I. Farnan, The effect of fission-energy Xe ion irradiation on dissolution of  $\text{UO}_2$  thin films, *J. Alloys Compd.* 721 (2017) 586–592.
- [14] K. Ollila, M. Olin, M. Lipponen, Solubility and oxidation state of uranium under anoxic conditions ( $\text{N}_2$  atmosphere), *Radiochim. Acta* 74 (1996) 9–13.
- [15] H. Blank, Properties of fission spikes in  $\text{UO}_2$  and UC due to electronic stopping power, *Phys. Status Solidi A* 10 (1972) 465–478.
- [16] P.B. Weisensee, J.P. Feser, D.G. Cahill, Effect of ion irradiation on the thermal conductivity of  $\text{UO}_2$  and  $\text{U}_3\text{O}_8$  epitaxial layers, *J. Nucl. Mater.* 443 (2013) 212–217.
- [17] N. Ishikawa, Y. Chimi, O. Michikami, Y. Ohta, K. Ohhara, M. Lang, R. Neumann, Study of structural change in  $\text{CeO}_2$  irradiated with high-energy ions by means of X-ray diffraction measurement, *Nucl. Instrum. Meth. Phys. Res. B* 266 (2008) 3033–3036.
- [18] H.J. Matzke, P.G. Lucuta, T. Wiss, Swift heavy ion and fission damage effects in  $\text{UO}_2$ , *Nucl. Instrum. Meth. Phys. Res. B* 166–167 (2000) 920–926.
- [19] H.J. Matzke, Radiation damage in nuclear materials, *Nucl. Instrum. Meth. Phys. Res. B* 65 (1992) 30–39.
- [20] H.J. Matzke, A. Turos, G. Linker, Polygonization of single crystals of the fluorite-type oxide  $\text{UO}_2$  due to high dose ion implantation, *Nucl. Instrum. Meth. Phys. Res. B* 91 (1994) 294–300.
- [21] T. Sonoda, M. Kinoshita, N. Ishikawa, M. Sataka, A. Iwase, K. Yasunaga, Clarification of high density electronic excitation effects on the microstructural evolution in  $\text{UO}_2$ , *Nucl. Instrum. Meth. Phys. Res. B* 268 (2010) 3277–3281.
- [22] V.G. Baranov, A.V. Lunev, A.V. Tenishev, A.V. Khulunov, Interaction of dislocations in  $\text{UO}_2$  during high burn-up structure formation, *J. Nucl. Mater.* 444 (2014) 129–137.
- [23] V.G. Baranov, A.V. Lunev, V.F. Reutov, A.V. Tenishev, M.G. Isaenkova, A.V. Khulunov, An attempt to reproduce high burn-up structure by ion irradiation of SIMFUEL, *J. Nucl. Mater.* 452 (2014) 147–157.
- [24] N. Nakae, H. Akiyama, H. Miura, T. Baba, K. Kamimura, S. Kurematsu, Y. Kosaka, A. Yoshino, T. Kitagawa, Thermal property change of MOX and  $\text{UO}_2$  irradiated up to high burnup of 74GWd/t, *J. Nucl. Mater.* 440 (2013) 515–523.
- [25] V.V. Rondinella, T. Wiss, The high burn-up structure in nuclear fuel, *Mater. Today* 13 (2010) 24–32.
- [26] M. Kinoshita, K. Yasunaga, T. Sonoda, A. Iwase, N. Ishikawa, M. Sataka, K. Yasuda, S. Matsumura, H.Y. Geng, T. Ichinomiya, Y. Chen, Y. Kaneta, M. Iwasawa, T. Ohnuma, Y. Nishiura, J. Nakamura, H.J. Matzke, Recovery and restructuring induced by fission energy ions in high burnup nuclear fuel, *Nucl. Instrum. Meth. Phys. Res. B* 267 (2009) 960–963.
- [27] C.T. Walker, D. Staicu, M. Sheindlin, D. Papaioannou, W. Goll, F. Sontheimer, On the thermal conductivity of  $\text{UO}_2$  nuclear fuel at a high burn-up of around 100MWd/kgHM, *J. Nucl. Mater.* 350 (2006) 19–39.
- [28] T. Sonoda, M. Kinoshita, I.L.F. Ray, T. Wiss, H. Thiele, D. Pellottiero, V.V. Rondinella, H.J. Matzke, Transmission electron microscopy observation on irradiation-induced microstructural evolution in high burn-up  $\text{UO}_2$  disk fuel, *Nucl. Instrum. Meth. Phys. Res. B* 191 (2002) 622–628.
- [29] N. Lozano, L. Desgranges, D. Aymes, J.C. Niepce, High magnification SEM observations for two types of granularity in a high burnup PWR fuel rim, *J. Nucl. Mater.* 257 (1998) 78–87.
- [30] J. Cobos, D. Papaioannou, J. Spino, M. Coquerelle, Phase characterisation of simulated high burn-up  $\text{UO}_2$  fuel, *J. Alloys Compd.* 271–273 (1998) 610–615.
- [31] I.L.F. Ray, H.J. Matzke, H.A. Thiele, M. Kinoshita, An electron microscopy study of the RIM structure of a  $\text{UO}_2$  fuel with a high burnup of 7.9% FIMA, *J. Nucl. Mater.* 245 (1997) 115–123.
- [32] H.J. Matzke, J. Spino, Formation of the rim structure in high burnup fuel, *J. Nucl. Mater.* 248 (1997) 170–179.
- [33] H.J. Matzke, M. Kinoshita, Polygonization and high burnup structure in nuclear fuels, *J. Nucl. Mater.* 247 (1997) 108–115.
- [34] H.J. Matzke, Oxygen potential in the rim region of high burnup  $\text{UO}_2$  fuel, *J. Nucl. Mater.* 208 (1994) 18–26.
- [35] H.J. Matzke, On the rim effect in high burnup  $\text{UO}_2$  LWR fuels, *J. Nucl. Mater.* 189 (1992) 141–148.
- [36] K. Opel, S. Weiß, S. Hübener, H. Zänker, G. Bernhard, Study of the solubility of amorphous and crystalline uranium dioxide by combined spectroscopic methods, *Radiochim. Acta* 95 (2007) 143–149.
- [37] H. He, R.K. Zhu, Z. Qin, P. Keech, Z. Ding, D.W. Shoesmith, Determination of local corrosion kinetics on hyper-stoichiometric  $\text{UO}_{2+x}$  by scanning electrochemical microscopy, *J. Electrochem. Soc.* 156 (2009) C87–C94.
- [38] N. Nakae, T. Koike, T. Kirihara, Electrical conductivity and thermoelectric power in irradiated  $\text{UO}_{2+x}$ , *J. Nucl. Mater.* 73 (1978) 217–221.
- [39] Z. Hiezl, D.I. Hambley, C. Padovani, W.E. Lee, Processing and microstructural characterisation of a  $\text{UO}_2$ -based ceramic for disposal studies on spent AGR fuel, *J. Nucl. Mater.* 456 (2015) 74–84.
- [40] H.J. Matzke, Radiation damage in crystalline insulators, oxides and ceramic nuclear fuels, *Radiat. Eff.* 64 (1982) 3–33.
- [41] H. Kleykamp, The chemical state of the fission products in oxide fuels, *J. Nucl. Mater.* 131 (1985) 221–246.

- [42] J.F. Ziegler, J.P. Biersack, M.D. Ziegler, The Stopping and Range of Ions in Matter, SRIM Co., Chester, Maryland, U.S.A., 2008.
- [43] T. Wiss, H.J. Matzke, C. Trautmann, M. Toulemonde, S. Klaumünzer, Radiation damage in  $\text{UO}_2$  by swift heavy ions, *Nucl. Instrum. Meth. Phys. Res. B* 122 (1997) 583–588.
- [44] E.S. Ilton, J.S. Pacheco, J.R. Bargar, Z. Shi, J. Liu, L. Kovarik, M.H. Engelhard, A.R. Felmy, Reduction of U(VI) incorporated in the structure of hematite, *Environ. Sci. Technol.* 46 (2012) 9428–9436.
- [45] E.J. Shchofield, H. Veeramani, J.O. Sharp, E. Suvorova, R. Bernier-Latmani, A. Mehta, J. Stahlman, S.M. Webb, L. Clark, S.D. Conradson, E.S. Ilton, J.R. Bargar, Structure of biogenic uraninite produced by *Shewanella oneidensis* strain MR-1, *Environ. Sci. Technol.* 42 (2008) 7898–7904.
- [46] D. Shirley, High-resolution x-ray photoemission spectrum of the valence bands of gold, *Phys. Rev. B* 5 (1972) 4709–4714.
- [47] D.J. Edwards, A.J. Popel, M.E. Bowden, I. Monnet, C. Grygiel, I. Farnan, TEM and XRD studies of  $\text{UO}_2$ -based simfuel irradiated with fission energy ions, (in preparation).
- [48] H. He, Z. Qin, D.W. Shoesmith, Characterizing the relationship between hyperstoichiometry, defect structure and local corrosion kinetics of uranium dioxide, *Electrochim. Acta* 56 (2010) 53–60.
- [49] A.J. Popel, V.A. Lebedev, P.G. Martin, A.A. Shiryayev, G.I. Lampronti, R. Springell, S.N. Kalmykov, T.B. Scott, I. Monnet, C. Grygiel, I. Farnan, Structural effects in  $\text{UO}_2$  thin films irradiated with fission-energy Xe ions, *J. Nucl. Mater.* 482 (2016) 210–217.
- [50] A.J. Popel, S. Le Sollic, G.I. Lampronti, J. Day, P.K. Petrov, I. Farnan, The effect of fission-energy Xe ion irradiation on the structural integrity and dissolution of the  $\text{CeO}_2$  matrix, *J. Nucl. Mater.* 484 (2017) 332–338.
- [51] Y.A. Teterin, A.J. Popel, K.I. Maslakov, A.Y. Teterin, K.E. Ivanov, S.N. Kalmykov, R. Springell, T.B. Scott, I. Farnan, XPS study of ion irradiated and unirradiated  $\text{UO}_2$  thin films, *Inorg. Chem.* 55 (2016) 8059–8070.
- [52] R.J. McEachern, P. Taylor, A review of the oxidation of uranium dioxide at temperatures below 400°C, *J. Nucl. Mater.* 254 (1998) 87–121.
- [53] S.A. Steward, E.T. Mones, Comparison and modeling of aqueous dissolution rates of various uranium oxides, *Mater. Res. Soc. Symp. Proc.* 465 (1997) 557–564.
- [54] E.M. Pierce, J.P. Icenhower, R.J. Serne, J.G. Catalano, Experimental determination of  $\text{UO}_2(\text{cr})$  dissolution kinetics: effects of solution saturation state and pH, *J. Nucl. Mater.* 345 (2005) 206–218.
- [55] P. Carbol, P. Fors, S. Van Winckel, K. Spahiu, Corrosion of irradiated MOX fuel in presence of dissolved  $\text{H}_2$ , *J. Nucl. Mater.* 392 (2009) 45–54.
- [56] P. Vitorge, H. Capdevila, S. Maillard, M.-H. Faure, T. Vercouter, Thermodynamic Stabilities of  $\text{MO}_{2+x}(\text{s})$  ( $M = \text{U}, \text{Np}, \text{Pu}$  and  $\text{Am}$ ), Pourbaix diagrams, *J. Nucl. Sci. Technol.* 39 (2002) 713–716.
- [57] V. Neck, J.I. Kim, Solubility and hydrolysis of tetravalent actinides, *Radiochim. Acta* 89 (2001) 1–16.